



On the growth, orientation and hardness of chemical vapor deposited Ti(C,N)

L. von Fieandt^{a,*}, K. Johansson^a, T. Larsson^b, M. Boman^a, E. Lindahl^c

^a Uppsala University, Department of Chemistry – Ångström Laboratory, Lägerhyddsvägen 1, Box 538, 75120 Uppsala, Sweden

^b Seco Tools AB, Björnbacksvägen 2, 73782 Fagersta, Sweden

^c AB Sandvik Coromant, Lerkrogsvägen 19, 12679 Hagersten, Sweden

ARTICLE INFO

Keywords:

CVD
Ti(C,N)
Hard coating
Thermodynamic modelling

ABSTRACT

Chemical vapor deposition (CVD) of Ti(C,N) from a reaction gas mixture of TiCl₄, CH₃CN, H₂ and N₂ was investigated with respect to gas phase composition and kinetics. The gas phase composition was modelled by thermodynamic calculations and the growth rate of the CVD process was measured when replacing H₂ for N₂ while the sum of partial pressures H₂ + N₂ was kept constant. The N₂/H₂ molar ratio was varied from 0 to 19. Single crystal c-sapphire was used as substrates. It was found that low molar ratios (N₂/H₂ molar ratio below 0.6) lead to an increased Ti(C,N) growth rate with up to 22%, compared to deposition without added N₂. The mechanism responsible for the increased growth rate was attributed to the formation and increased gas phase concentration of one major growth species, HCN, in the gas phase. The texture of the Ti(C,N) films were also studied. <211> textured layers were deposited at N₂/H₂ molar ratios below 9. At higher molar ratios, <111> oriented Ti(C,N) layers were deposited and the grain size increased considerably. The films deposited at a N₂/H₂ ratio above 9 exhibited superior hardness, reaching 37 GPa. The increased hardness is attributed to an almost epitaxial orientation between the layer and the substrate. The absence of grain twinning in the <111> oriented layer also contributed to the increased hardness. The Ti(C,N) layers were characterized by elastic recoil detection analysis, X-ray photo electron spectroscopy, scanning electron microscopy, X-ray diffraction and nanoindentation.

1. Introduction

Modern chip forming metal cutting applications set a very high demand on the wear resistance of cutting tools. To increase the wear resistance, hard protective coatings are used. Depending on the application, the tool is coated using chemical vapor deposition (CVD) and/or physical vapor deposition (PVD). The coatings are optimized to meet a variety of different cutting applications and materials. Today the trend in the field of metal cutting is to use higher cutting speeds, but also to extend the use of the tools to materials that are difficult to machine.

State of the art cutting tools are coated with a layer combination of TiN/Ti(C,N)/Al₂O₃ with the TiN/Ti(C,N) layers being closest to the substrate. The alumina layer has continuously been optimized with respect to phase control (α or κ -Al₂O₃) and texture, e.g. (001) thereby increasing the lifetime of this type of coated tool considerably [1–3]. However, texture control has mainly been optimized on the alumina layer and a similar optimization of texture and growth direction of the intermediate Ti(C,N) layer has so far almost been overlooked.

Titanium carbonitride, Ti(C,N), has been used as a wear resistant

coating material for WC/Co cutting tools since the beginning of the 1970s [4]. Initially the coatings were deposited from TiCl₄-CH₄-N₂ reaction gas mixtures at relatively high temperatures, around 1000 °C [5,6]. At such high deposition temperatures problems with decarburization of the tool material can arise, causing formation of brittle carbon deficient phases (η -phase; M₆C or M₁₂C, M = W,Co). The introduction of moderate temperature (MT) CVD enabled deposition of Ti(C,N) at a temperature as low as 700 °C due to the use of the more reactive precursor CH₃CN instead of CH₄ and N₂. The lower deposition temperature reduced the problem of decarburization and η -phase formation [4,5]. Despite the long use of the MT CVD-Ti(C,N) process in the cutting tool industry, the mechanisms involved in the deposition process are not particularly well understood.

Ti(C,N) coatings deposited using the MT process (CH₃CN + TiCl₄ + H₂) generally grow columnar with a <311>/<211> out of plane orientation [7–12]. The morphology of the MT-Ti(C,N) can be altered by changing the TiCl₄/CH₃CN ratio. While this change affects the morphology, the orientation of the grains remains unaffected [13].

Most cutting tools are coated with multi-layer coatings of Ti(C,N)

* Corresponding author.

E-mail address: linus.fieandt@kemi.uu.se (L. von Fieandt).

<http://dx.doi.org/10.1016/j.tsf.2017.10.037>

Received 10 April 2017; Received in revised form 9 October 2017; Accepted 18 October 2017

Available online 19 October 2017

0040-6090/© 2017 The Authors. Published by Elsevier B.V. This is an open access article under the CC BY-NC-ND license (<http://creativecommons.org/licenses/by-nc-nd/4.0/>).

and Al_2O_3 . The adhesion between the layers in the multi-layer system is crucial for a high performance tool. Layer adhesion is affected by the orientation relation between different layers, where a large mismatch between two layers can cause a poor adhesion due to a high amount of strain over the interface. The orientation relation between TiC/TiN deposited onto $\alpha\text{-Al}_2\text{O}_3$ has been investigated previously [14,15], showing the epitaxial relation $(111)\text{TiC}/\text{TiN}||(\text{001})\alpha\text{-Al}_2\text{O}_3$. Epitaxial growth is observed despite the relatively large mismatch between layer and substrate. However, no published work on the orientation relation between MT-Ti(C,N) deposited onto (001) oriented $\alpha\text{-Al}_2\text{O}_3$ are known to the authors. In previous studies the carbon/nitrogen precursors for TiC/TiN were CH_4 and N_2 , respectively and layers were grown at significantly higher temperatures. The assumed CVD reaction path for Ti containing layers using TiCl_4 suggests that presence of hydrogen reduces the energy requirement of Cl^- removal from TiCl_4 [16,17]. This is achieved through the formation of HCl instead of Cl_2 . As most MT-Ti(C,N) are deposited in excess of H_2 , the Cl^- removal is considered as a fast reaction and not as the rate determining step of Ti(C,N) formation. The assumed rate determining step is the cleavage of the $\text{C}\equiv\text{N}$ bond in the CH_3CN , which, due to its high bond strength, requires more energy than Cl^- removal from TiCl_4 [18].

N_2 is sometimes added to the reaction gas mixture during deposition of MT-Ti(C,N) as it is believed to improve adhesion and a more homogeneous coating thickness distribution. Furthermore, N_2 is known to increase the deposition rate, however, the mechanism has not been investigated [13]. The reactivity of N_2 in a reaction gas mixture consisting of TiCl_4 , CH_3CN and H_2 at temperatures of typically 800–900 °C is low and will therefore not affect the coating composition [10,19,20]. Studies of TiN coatings grown from TiCl_4 and NH_3 at (600–900 °C) indicate that added N_2 affects the microstructure, orientation and growth rate of the deposit [21,22]. The authors discuss whether N_2 changes the growth and surface chemistry by adsorption of N_2 , leading to surface blockage. Also the stability of NH_3 as a function of added N_2 was discussed. The effect of N_2 addition on growth of MT-Ti(C,N) layers has not been studied.

In this paper the H_2/N_2 ratio in the CVD reaction forming Ti(C,N) has been varied in a systematic way, both experimentally and theoretically, in order to study the effects on orientation, orientation relationships, microstructure, growth kinetics and hardness of the MT-Ti(C,N) layer.

2. Experimental details

2.1. CVD deposition

Ti(C,N) was grown on polished $10 \times 10 \times 0.5$ mm single crystal c-sapphire (001) substrates with a surface roughness $< 5 \text{ \AA}$ supplied by MTI corp. A Bernex 325 hot wall CVD reactor was used and the sapphire substrates were placed at half the tray radius and half the reactor height. Furthermore, 3 polished WC-Co control pieces were placed at the center, half radius and at the periphery of bottom, middle and top levels of the reactor, respectively. The process conditions are shown in

Table 1
Ti(C,N) deposition parameters. $T = 830 \text{ °C}$, $P_{\text{tot}} = 8 \text{ kPa}$, $\text{TiCl}_4 = 0.26 \text{ kPa}$, $\text{CH}_3\text{CN} = 0.04 \text{ kPa}$.

Sample	H_2 (kPa)	N_2 (kPa)	Ar(kPa)	Deposition time (min)	Growth rate ($\mu\text{m/h}$)
0	7.7	0	0	70	1.24
1	6.5	1.2	0	60	1.52
1A	6.5	0	1.2	80	1.01
2	4.9	2.8	0	70	1.43
3	2.8	4.9	0	70	1.16
4	0.7	7.0	0	150	0.67
5	0.4	7.3	0	360	0.24

Table 1.

In the experiments, excess hydrogen was reduced and replaced with nitrogen in a stepwise approach as shown in Table 1. Argon was used instead of N_2 in one experiment (sample 1A), this sample was only characterized with respect to the growth rate. The total gas flow was kept constant at 2400 l/h in all the depositions. Deposition times were adjusted in order to deposit layers of equal thicknesses (about 1.5 μm).

2.2. Thermodynamic modelling

In order to increase the understanding of the deposition process and the main growth species, thermodynamic modelling was employed. The gas phase composition at the process conditions presented in Table 1 was modelled by thermodynamic calculations. A free-energy minimization technique was used (Program: Ekvicalc) [23]. TiCl_4 , CH_3CN , N_2 , H_2 and Ar were used as reactants in the calculations. For an accurate estimation of the gas phase composition prior to deposition all condensed phases were suppressed in the calculations and a total of 69 gaseous species were used in the calculations (for a complete list see Appendix A, Table A1). This is a common approach to model gas phase reactions in CVD [24]. Thermodynamic calculations can predict a chemical system only if the chemical reactions can reach equilibrium. Since gas phase reactions at 830 °C are fast, the gases are preheated and mixed at an earlier stage in the reactor and the residence time of the gas phase in the reactor is long (about 2–3 s depending on the total pressure), this approximation can be used. The results in this investigation were used to clarify the experimental results by modelling which gas phase species are most abundant and most likely the main contributor to the growth of a CVD coating.

2.3. Characterization

The crystallography of the thin films, phase compositions and the out-of-plane orientations were evaluated by θ – 2θ X-ray diffraction using a Philips MRD-XPRT diffractometer equipped with a primary hybrid monochromator and a secondary X-ray mirror. In addition, pole figures in the Ψ range 6–89° were acquired using a Philips MRD-XPRT diffractometer operating in point focus mode and equipped with a primary X-ray poly-capillary lens with crossed slits, a secondary flat graphite monochromator with parallel plate collimator, and a nickel filter. Cu $K\alpha$ -radiation was used for all X-ray measurements. The pole figure measurements were performed on the Ti(C,N) (200) diffraction peak, i.e. at 42.1° in 2θ . In addition to the pole figure measurements the poly-capillary set-up was used to determine residual stresses in the layers. The stress states were calculated using the cell parameters determined from (111) planes parallel to the surface and (422) planes 90° from the surface. The stress was calculated with Hooks law using the elastic modulus from the hardness measurements described below [25].

Top surface morphologies, cross section film thicknesses and microstructures were examined using a Zeiss Merlin High resolution scanning electron microscope (HR-SEM) operated at an acceleration voltage of 3 kV.

The compositions were investigated by X-ray photoelectron spectroscopy (XPS) using a PHI-Quantum 2000 scanning ESCA microprobe with monochromatic Al $K\alpha$ radiation. For all layers, sputtered depth profiles were acquired to determine the average bulk composition. The profiles were attained by 4 kV Ar^+ ions on areas of $1 \times 1 \text{ mm}^2$. The compositions were determined using sensitivity factors for Ti, C and N, obtained from reference measurements of two Ti(C,N) samples by elastic recoil detection analysis (ERDA). Calibration allowed atomic concentration to be determined within 0.4% at.

Mechanical evaluation through nanoindentation was performed using a CSM UNHT Nanoindenter with a Berkovich tip diamond indenter. The indentations were made at a constant linear loading of 3 mN/min to a depth of 110 nm. Hardness was measured after gentle surface polishing (with 6 μm diamond slurry) to decrease the surface

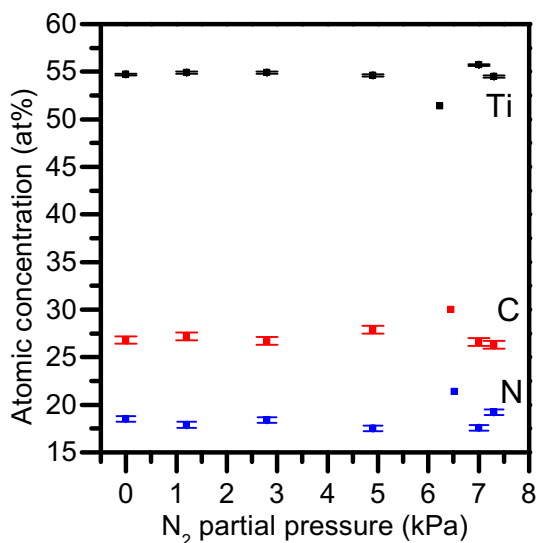


Fig. 1. Composition of all deposited Ti(C,N) layers as a function of N₂ partial pressure. Ti, C and N are marked in black, red and blue respectively. Error bars represent one standard deviation. (For interpretation of the references to colour in this figure legend, the reader is referred to the web version of this article.)

roughness. The hardness was calculated using the method presented by Oliver and Pharr and 36 indentations were made and the average value was considered the coating hardness [26]. Equipment reference measurements were performed on fused silica between the measurements to ensure optimal indenter performance.

3. Results and discussion

3.1. Compositional analysis (XPS)

To correctly interpret the growth rate and kinetics of CVD Ti(C,N) it is important to investigate if the composition of the deposit varies with the experimental parameters. The C/N ratio in Ti(C,N) was therefore quantified by XPS as a function of the H₂/N₂ partial pressures. The results are shown in Fig. 1. Only Ti, C and N were observed; all other elements were below the detection limit of the XPS technique, i.e. below 1% (at).

Despite the introduction of large amounts of N₂ to the gas phase the average bulk composition for each layer was almost constant, see Fig. 1. Only a slight increase in the N content can be observed in the coating grown at the highest N₂ partial pressure (7.3 kPa).

It can also be observed that the relation between Ti and the non-metal content is not 1:1. The ratio [Ti]/([C] + [N]) varies between 1.20 and 1.26 for all layers, indicating that the composition of the Ti(C,N) coating was slightly over-stoichiometric with respect to Ti. The C/N molar ratio was 1.6 for the layers deposited with p_{N2} below 7.3 kPa. This is in agreement with a previous study of Ti(C,N) deposited using MT-CVD [10].

3.2. Thermodynamic calculations and growth kinetics

The growth rate of Ti(C,N) from TiCl₄, CH₃CN and H₂ at 830 °C and at different partial pressures of H₂ and N₂ is shown in Fig. 2. Here H₂ is replaced by N₂, keeping a constant total pressure of 8 kPa. The partial pressures of TiCl₄ and CH₃CN were kept constant at 0.26 and 0.040 kPa, respectively. It can be seen that the growth rate of Ti(C,N) was strongly affected when increasing the partial pressure of N₂. When increasing p_{N2} from 0 to 1.2 kPa the growth rate increases from 1.24 to a maximum of 1.52 μm/h. When further increasing the N₂ partial pressure the growth rate decreases continuously down to 0.25 μm/h at a N₂ partial pressure of 7.3 kPa.

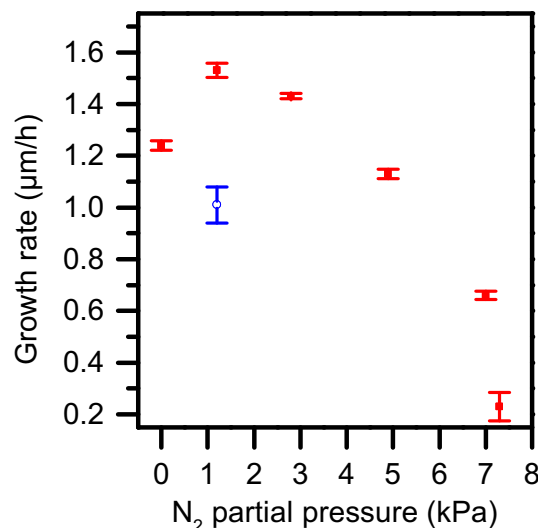


Fig. 2. Growth rate of Ti(C,N) as a function of N₂ partial pressure. Growth rate for N₂ replaced by argon is marked with a hollowed out blue circle. Error bars represent one standard deviation. (For interpretation of the references to colour in this figure legend, the reader is referred to the web version of this article.)

The layer thickness distribution evaluated through cross section measurements on the WC-Co control pieces gave a similar profile at all N₂ partial pressures, however, the spread in layer thickness decreased upon N₂ addition. Above 2.8 kPa N₂ partial pressure there was no observed further decrease of the spread in layer thickness. These observations are in agreement with the suggestions stated previously [13].

In order to investigate the mechanism behind the observed growth rate increase, thermodynamic calculations of the gas phase composition were made using the same parameters as in the experiments. Fig. 3 shows the partial pressures of the most abundant reaction products from a reaction gas mixture of TiCl₄, CH₃CN, H₂ and N₂ at 830 °C. In the calculations the initial amount of TiCl₄ and CH₃CN were constant at 0.26 and 0.04 kPa respectively and the amount of H₂ and N₂ was varied in such a way that the sum of partial pressures of the gases was constant (8 kPa).

The partial pressures of gas phase species can be seen in Fig. 3, and

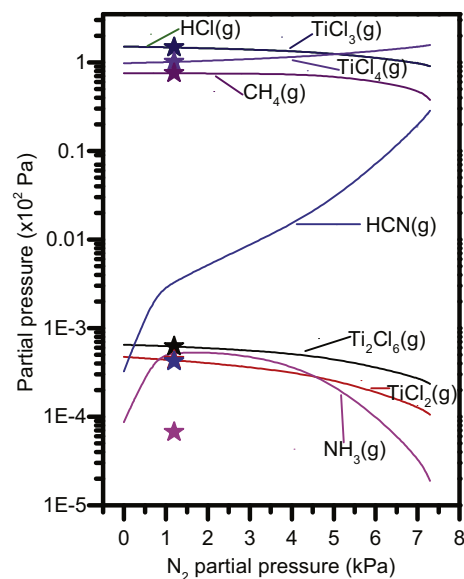


Fig. 3. Gas phase equilibrium content, calculated with the same parameters as used in the experiments. All species are as a function of N₂ partial pressure. Stars of respective colour represent calculations where Ar is added instead of N₂.

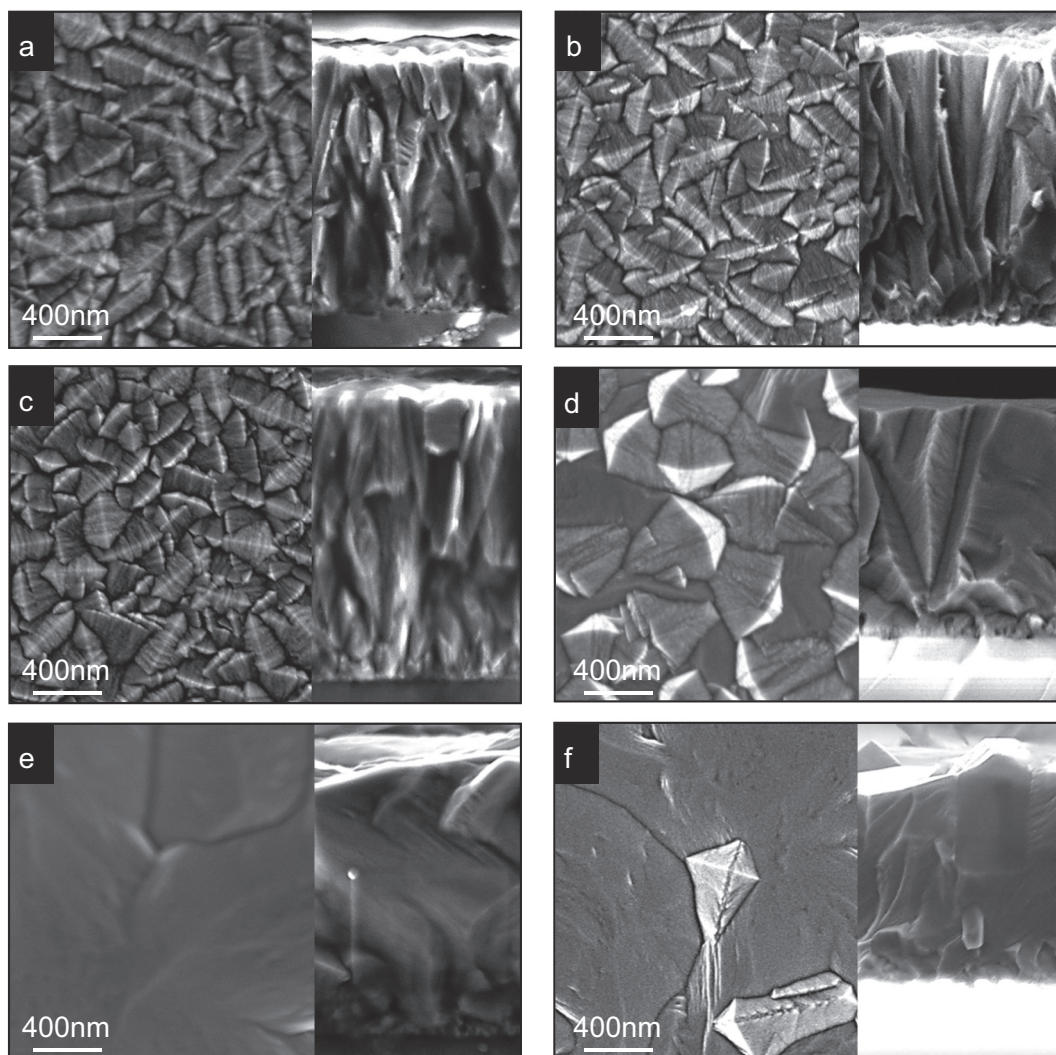


Fig. 4. SEM micrographs of samples 0–5, 0–7.3 kPa N₂ (a–f) showing top view morphologies and cross-section microstructures.

only molecules with partial pressure above 10^{-3} Pa were included (66 gas species were used in the calculations, see Table A1, Appendix A). From Fig. 3 it is shown that the main carbon and nitrogen containing species are CH₄, HCN and NH₃. Of the three, NH₃ is formed in the lowest amount but reaches a maximum (0.54 Pa) at a N₂ partial pressure of 1.2 kPa. The amount of CH₄ is almost constant and is 3–4 orders of magnitude higher than NH₃ in the entire pressure range investigated. The partial pressure of HCN increases rapidly with increasing p_{N₂} and is of the same order as CH₄ at the highest N₂ partial pressure. This makes HCN the most likely major contributor to both carbon and nitrogen in the CVD process. Since the Ti(C,N) layer contains more carbon than nitrogen, it is unlikely that NH₃ does form in significant amounts, as it would increase the N content of the layer and form pure TiN. Which leads to the conclusion that the conversion of CH₃CN to NH₃ is kinetically limited, and thereby not accounted for in the thermodynamic calculations.

An additional calculation was made at the growth rate maxima of 1.2 kPa N₂, where N₂ was replaced by Ar. The result is included in Fig. 3 and is represented by star points. The partial pressure of HCN is reduced by almost one order of magnitude. The other reaction products were unaffected by the Ar replacement. This means that N₂ increases HCN partial pressure and this can explain the initial increase in growth rate when H₂ is replaced by N₂.

The observed growth rate decrease upon further increase of the N₂ partial pressure is believed to be caused by the reduced partial pressure

of TiCl₃ (Fig. 3). Instead the partial pressure of TiCl₄ increases as the amount of H₂ decreases. Hydrogen is needed for the removal of Cl by forming HCl and when the amount of H₂ is reduced the amount of HCl is also reduced and the amount of TiCl₄ increases, thereby decreasing the growth rate.

Hydrogen is also needed to form HCN and CH₄ from CH₃CN. The reaction gas mixture switches from an excess of H₂ to a depletion of hydrogen when p_{N₂} is increased and, as a result, the growth rate decreases. One of the main conclusions from the calculations are the most probable growth species for CVD of Ti(C,N). The main Ti containing species in the gas phase is TiCl₃ (except for the highest N₂ partial pressures), and HCN for C and N. CH₄ may also contribute to C in the deposited Ti(C,N). Possibly NH₃ may contribute at N₂ partial pressures of below 1.5 kPa where NH₃ is only about one order of magnitude lower than HCN. However, a contribution from NH₃ would lead to an increased N content in the Ti(C,N) layers, which was not the case for the layers deposited at a p_{N₂} below 7.3 kPa.

3.3. Morphology and microstructure

Fig. 4 shows the morphology and cross section of samples 0–5 in Table 1. Fig. 4a–c shows that layers deposited at p_{N₂} ≤ 2.8 kPa attained grain morphologies similar to what has been reported previously for MT-Ti(C,N) coated WC/Co substrates [10,11]. This morphology was attributed to a <211> out of plane orientation. The layer grown at

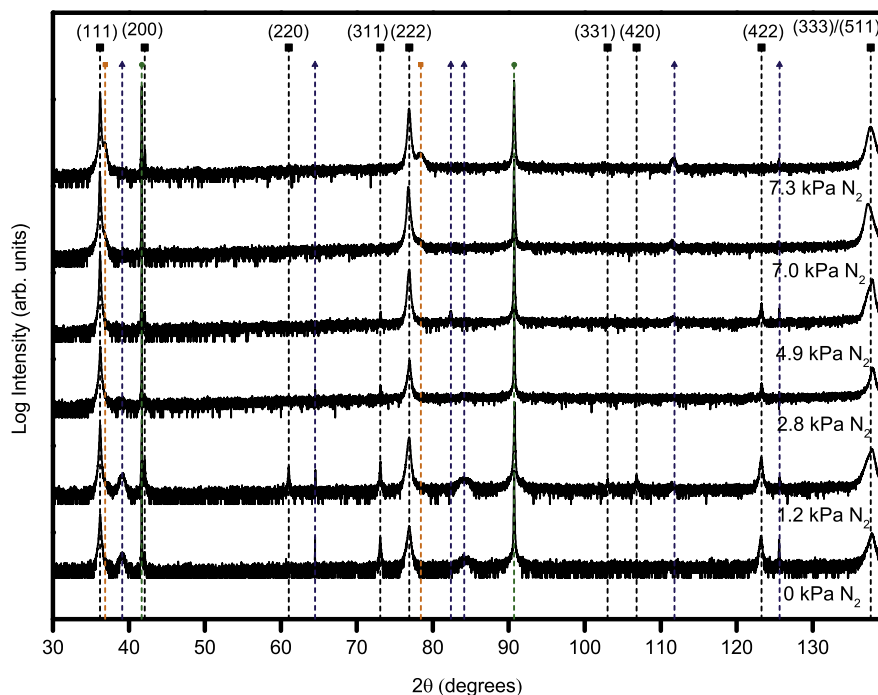


Fig. 5. θ - 2θ diffractograms of samples 0–5 (0–7.3 kPa N_2). Ti (C,N) peaks are marked with (hkl), TiN peaks indicated by orange squares, instrument artifacts (Al from the sample holder) indicated by blue triangles, and sapphire (006) and (0012) peaks indicated by green circles. (For interpretation of the references to colour in this figure legend, the reader is referred to the web version of this article.)

4.9 kPa N_2 has a mixture of two morphologies, large flat grains and coarse ridge like grains, Fig. 4d. The layer grown at 7 kPa N_2 partial pressure, shown in Fig. 4e, shows a homogeneous surface morphology with large flat grains. With further increase of N_2 partial pressure to 7.3 kPa the surface morphology, Fig. 4f, is inhomogeneous with a mixture of large flat grains and ridge like grains as the ones observed for the lower N_2 partial pressures. Layers deposited at a N_2 partial pressure above 2.8 kPa showed an increased grain size compared to layers grown at N_2 partial pressures \leq 2.8 kPa. The lower growth rate of layers deposited above 2.8 kPa N_2 partial pressure allows larger grains to form.

Fig. 4a–f also show the cross sections of the layers, showing that the layers deposited with $p_{N_2} \leq$ 2.8 kPa (Fig. 4a–c) have a fibrous microstructure consistent with previously reported layers with ridge like morphology and $\langle 211 \rangle$ orientation [9–12,27]. The layers deposited with N_2 partial pressures between 4.9 and 7.3 kPa have a non-fibrous, more compact microstructure (Fig. 4d–f). The more compact microstructure is associated with the larger grains.

3.4. Orientation and phase analysis

Fig. 5 shows θ - 2θ diffractograms of all deposited layers. It can be seen that all layers have a Ti(C,N) with a dominant $\langle hhh \rangle$ orientation. Due to the absolute overlap between the (511) peak and the (333) peak a $\langle 511 \rangle$ orientation cannot be excluded. The layers deposited with p_{N_2} below 7 kPa has additional orientations present ($\langle 100 \rangle$, $\langle 110 \rangle$, $\langle 311 \rangle$ and $\langle 211 \rangle$). The layers deposited at 7 and 7.3 kPa N_2 , exhibit only $\langle hhh \rangle$ and possibly $\langle 511 \rangle$ orientations.

The layers deposited at $p_{N_2} \leq$ 7 kPa only show peaks from Ti(C,N) corresponding to a unit cell $a = 4.29 \text{ \AA}$, whereas the layer deposited at 7.3 kPa p_{N_2} show additional peaks which correspond to TiN with a unit cell of $a = 4.22 \text{ \AA}$, calculated from the (hhh) peaks of respective phase. Despite the complete miscibility of the two phases TiC and TiN it is evident from the θ - 2θ diffractogram that a co-deposition of two separate phases has taken place [28]. This co-deposition of TiN and Ti(C,N) is most probably caused by the high N_2 partial pressure and the low growth rate of Ti(C,N). The intensities of the TiN peaks compared to the Ti(C,N) peaks are much lower, thus indicating a much smaller amount of TiN. This can be expected since CH_3CN is more reactive than N_2 at this temperature. The observation of a TiN phase for the layer deposited

at 7.3 kPa N_2 could correspond to the slight increase in N_2 content found by XPS, see Fig. 1.

The in-plane relationships of the different layer orientations were determined from pole figure measurements of the Ti(C,N)(200) pole, see Fig. 6a–f. All layers deposited at p_{N_2} below 7 kPa (samples 0–3) show pole figures exhibiting three sets of reflections. One set of reflections at a Ψ of 15.8° (marked d1) and 78.9° corresponding to a $\langle 511 \rangle$ out-of-plane orientation. A second set of reflections at a Ψ of 54.7° corresponding to a $\langle 111 \rangle$ out-of-plane orientation (marked d2). A third set of reflections corresponding to a $\langle 211 \rangle$ out-of-plane orientation observed at Ψ 35.3° and 65.9° (marked d3).

The layer orientation in sample 4, deposited at 7 kPa N_2 differs from the other deposited layers, in that it shows a pole figure (Fig. 6e) with only one set of reflections at a Ψ of 54.7° corresponding to a $\langle 111 \rangle$ out-of-plane orientation (marked d2). The layer deposited at the highest N_2 partial pressure, 7.3 kPa (sample 5), shows a pole figure (Fig. 6f) with only two sets of reflections. One set of very low intensity reflections at a Ψ of 15.8° and 78.9° (marked d1), corresponding to a $\langle 511 \rangle$ out-of-plane orientation, and one set at a Ψ of 54.7° , corresponding to a $\langle 111 \rangle$ out-of-plane orientation (marked d2). All observed orientations show crystal twinning (the number of observed reflections is doubled). The twinning is a result of a stacking fault in the Ti(C,N) deposition, where two different stacking sequences (ABC and CBA) cause a 180° rotation of the crystal axis. The twin domains are marked with td1 for $\langle 511 \rangle$, td2 for $\langle 111 \rangle$ and td3 for $\langle 211 \rangle$ respectively in Fig. 6a–e. $\langle 111 \rangle$ twinning was observed previously when TiC was deposited onto single crystal c-sapphire [29].

The reflections from the $\langle 211 \rangle$ orientation have larger broadening in both Ψ and Φ , indicating a lower degree of in-plane orientation compared to the reflections from the $\langle 111 \rangle$ and $\langle 511 \rangle$ orientations respectively. The morphology observed in Fig. 4a–d (samples 0–3, 0–4.9 kPa N_2), which is attributed to the $\langle 211 \rangle$ orientation in earlier studies, indicates that the $\langle 211 \rangle$ oriented part of the layer grows on top of the $\langle 111 \rangle$ oriented part. A nucleation on a less oriented surface will give a lower degree of in-plane orientation, thereby explaining the broadening of the $\langle 211 \rangle$ peaks observed in Fig. 6a–d.

Furthermore, by measuring a pole figure on the sapphire substrate, the in-plane relationship between substrate and the dominant $\langle 111 \rangle$ orientation could be determined as follows: $Al_2O_3(001)[110]/Ti(C,N)(111)[1-$

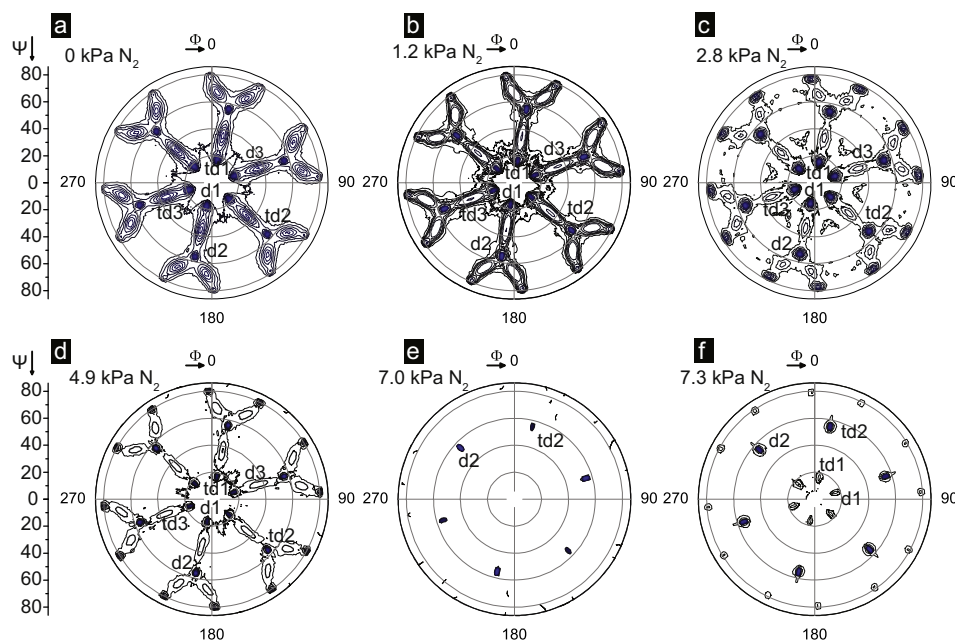


Fig. 6. Ti(C,N)(200) pole figures of samples deposited at p_{N_2} between 0 and 7.3 kPa (samples 0–5) represented in a–f respectively. All samples show evidence of crystal twinning, hence the six-fold symmetry.

21] for one of the twin domains (d2), and $Al_2O_3(00l)[-1-10]/Ti(C,N)(111)[-12-1]$ for the other twin domain (td2). This relation is in agreement with earlier studies of ccp metal deposited on $(00l)Al_2O_3$ [30]. The mismatch between the sapphire substrate and the layer were calculated for the experimentally determined in-plane orientation to be 10.3% along the $Al_2O_3[110]$ and 10.4% along the $Al_2O_3[-110]$ directions.

The in-plane relationship between the $\langle 111 \rangle$ oriented part of the layer and the weak $\langle 211 \rangle$ orientation in samples 0–3 was determined to be $Ti(C,N)(111)[01-1]/Ti(C,N)(211)[01-1]$ for one of the twin domains (d3), and $Ti(C,N)(111)[0-11]/Ti(C,N)(211)[0-11]$ for the other domain (td3). The in-plane relationship between the $\langle 511 \rangle$ orientation and the substrate could be determined as $Al_2O_3(00l)[110]/Ti(C,N)(511)[110]$ for one of the twin domains (d1), and $Al_2O_3(00l)[-1-10]/Ti(C,N)(511)[-1-10]$ for the other twin domain (td1).

The pole figures and the $\theta-2\theta$ measurements show that an increase of nitrogen partial pressure makes the layer more prone to grow in an orientation dictated by the substrate. This indicates that the orientation of Ti(C,N) can be controlled by the substrate or preceding layer orientation, when an appropriate process is used.

3.5. Nanoindentation

The hardness for all deposited layers was measured by nanoindentation. The trends in hardness are shown in Fig. 7. As can be seen, the layers deposited at N_2 partial pressures between 7 and 7.3 kPa (samples 4 and 5) exhibit a higher hardness, 37 ± 3 and 36 ± 3 GPa respectively, than those layers deposited at lower N_2 partial pressures. The hardness of samples grown with the highest N_2 partial pressure (samples 4 and 5) exceeds the previous reported hardness of MT-CVD-Ti(C,N), which is typically in the region 22–24 GPa [7–9,11,12,31]. The difference in microstructure, morphology and orientation between the layers deposited between 0 and 4.9 kPa N_2 partial pressure and the layers deposited between 7 and 7.3 kPa N_2 partial pressure will cause a difference in deformation behavior. The layers deposited between 7 and 7.3 kPa N_2 are oriented in only $\langle 111 \rangle$ (and $\langle 511 \rangle$) for the layer at 7.3 kPa N_2 , thereby maintaining the orientation relation with the substrate throughout the entire layer.

3.6. Stress measurements

The layer residual stresses were determined through measurement

of the cell parameter parallel to the surface and 90° to the surface. For the layer deposited with no N_2 the residual stress was calculated to be 0.21 GPa tensile, using the elastic modulus obtained through nanoindentation (632 GPa). The residual stress of the layer deposited with 7 kPa N_2 was compressive and calculated to 1.6 GPa, the elastic modulus (600 GPa) obtained in the nanoindentation was used in the calculation. The state of compressive stress in the layer deposited with 7 kPa N_2 could be a contributor to the increased hardness.

4. Conclusions

In the present work the growth rate, morphology, microstructure, orientation, hardness and composition of CVD Ti(C,N) was investigated as a function of the experimental gas phase composition. $TiCl_4$, CH_3CN , H_2 and N_2 were used as the reaction gas mixture. The gas phase composition was also modelled by thermodynamics calculations. The main active growth species in the gas were found to be $TiCl_3$ and HCN. When replacing H_2 by N_2 , the growth rate first increased then decreased again. The increase in growth rate was attributed to an increase of HCN and the latter to the decrease of $TiCl_3$.

The morphology and orientation could be tailored from fine grained

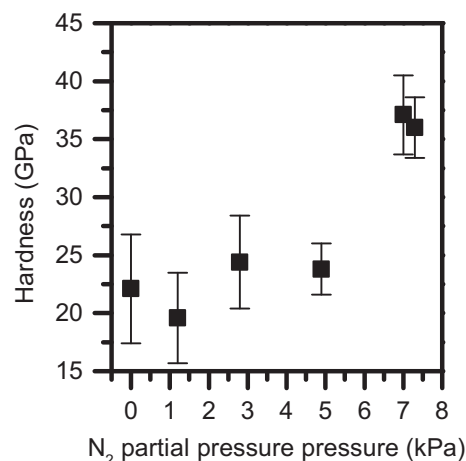


Fig. 7. Hardness as a function of N_2 partial pressure. Error bars represents one measurement standard deviation.

<211> to large grained <111> by adjusting the H₂ partial pressure. The modified morphology and orientation cannot be attributed to an altered composition, as only minor fluctuations were measured by XPS. For layers grown at a N₂/H₂ ratio below 18.25 the Ti(C,N) layer composition was constant. However, at the highest N₂ partial pressure, 7.3 kPa, co-deposition of TiN occurred.

The orientation relation between c-sapphire and Ti(C,N) was investigated by XRD and determined to be Al₂O₃(00l)[110]//Ti(C,N)(111)[1-21]. This relation gives rise to a relatively large mismatch of 10%. The orientation relation between the <111> oriented and <211> oriented Ti(C,N) was determined to be Ti(C,N)(111)[01-1]//Ti(C,N)(211)[01-1].

As a result of orientation and microstructure control, the hardness of the Ti(C,N) coating could be increased from 22 GPa to 37 GPa, which is the highest value measured for this type of coating. The highest hardness was observed for layers grown with a N₂/H₂ ratio higher than 9

(N₂ partial pressure ≤ 7 kPa). The slight compressive stresses in the layers deposited at N₂ partial pressures 7 and 7.3 kPa could partially explain the increased hardness. Possibilities to tune the layer hardness enable prerequisites to tailor the coated tool to suit different metal cutting operations.

Acknowledgements

Funding of CVD 2.0 by the Swedish Foundation for Strategic Research via SSF contract RMA15-0048 is gratefully acknowledged. Funding from Sandvik AB is gratefully acknowledged. Financial support of the Tandem Laboratory infrastructure by the Swedish Research Council via VR-RFI contract C0514401 and by the Swedish Foundation for Strategic Research via SSF contract RIF14-0053 is gratefully acknowledged.

Appendix A

Table A1

Substances used in the thermodynamic calculation with respective reference.

Reference [32]	Reference [33]	Reference [34]
H2(g)	C3H3N(g)	CH3CN(g)
N2(g)		CH3NC(g)
CH4(methane)	Reference [35]	CH3NH2(g)
HCN(g)	C2N(g)	HN3(g)
NH3(g)	CN2(g)	CH3N2H3(g)
H(g)	N3(g)	CHClCCl2(g)
C2H2(ethyne)	CH3Cl(g)	CH2CCl2(g)
C2H4(ethene)		CHClCHCl(g)
CH3(methyl)	Reference [36]	CHCl2CHCl2(g)
NH2(g)	TiCl4(g)	CHCl2CH2Cl(g)
C2N2(g)	Ti2Cl6(g)	CH3CHCl2(g)
CN(g)		C2H5Cl(g)
CH2(methylene)	Reference [37]	
C2N(g)	CHCl(g)	Reference [38]
N(g)	CH2Cl(g)	C2H6(ethane)
N2H2(g)	CH2Cl2(g)	C3H4(propyne)
N2H4(g)	CHCl3(g)	C3H4(propadiene)
CH(methylidene)	CNCl(g)	C3H6(propene)
C(g)		C3H6(cyclopropane)
N3(g)	Unlisted	C3H8(propane)
C3(g)	CCl3CN(g)	Reference [39]
C2(g)		Ar(g)
CCl(g)		
CCl2(g)		
CCl3(g)		
CCl4(g)		
C2Cl2(g)		
C2Cl4(g)		
C2Cl6(g)		
Cl(g)		
Cl2(g)		
HCl(g)		
TiCl(g)		
TiCl2(g)		

References

- [1] S. Rупpi, Enhanced performance of α-Al₂O₃ coatings by control of crystal orientation, Surf. Coat. Technol. 202 (2008) 4257–4269, <http://dx.doi.org/10.1016/j.surfcoat.2008.03.021>.
- [2] R. M'Saoubi, S. Rупpi, Wear and thermal behaviour of CVD α-Al₂O₃ and MTCVD Ti(C,N) coatings during machining, CIRP Ann. Manuf. Technol. 58 (2009) 57–60, <http://dx.doi.org/10.1016/j.cirp.2009.03.059>.
- [3] M. Fallqvist, S. Rупpi, M. Olsson, M. Ottosson, T.M. Grehk, Nucleation and growth of CVD α-Al₂O₃ on Ti_xO_y template, Surf. Coat. Technol. 207 (2012) 254–261, <http://dx.doi.org/10.1016/j.surfcoat.2012.06.087>.
- [4] R. Bonetti, H. Wiprächtiger, E. Mohn, CVD of titanium carbonitride at moderate temperature: Properties and applications, Met. Powder Rep. (1990) 837–840.
- [5] E. Kübel, New developments in chemically vapour-deposited coatings from an industrial point of view, Surf. Coat. Technol. 49 (1991) 268–274, <http://dx.doi.org/10.1016/j.surfcoat.1991.03.001>.

- 10.1016/0257-8972(91)90067-7.
- [6] S. Rупpi, B. Hgrelius, M. Huhtiranta, Wear characteristics of TiC, Ti (C,N), TiN and Al₂O₃ coatings in the turning of conventional and Ca-treated steels, *Int. J. Refract. Met. Hard Mater.* 16 (1998) 353–368.
- [7] A. Paseuth, H. Fukui, K. Yamagata, Surface & coatings technology improvement of mechanical properties and cutting performance of modified MT-TiC_xN_{1-x} coating by moderate temperature chemical vapor deposition, *Surf. Coat. Technol.* 291 (2016) 54–61, <http://dx.doi.org/10.1016/j.surfcoat.2016.02.023>.
- [8] A. Paseuth, H. Fukui, S. Okuno, H. Kanaoka, Y. Okada, Microstructure, mechanical properties, and cutting performance of TiC_xN_{1-x} coatings with various x values fabricated by moderate temperature chemical vapor deposition, *Surf. Coat. Technol.* 260 (2014) 139–147, <http://dx.doi.org/10.1016/j.surfcoat.2014.09.068>.
- [9] H. Holzschuh, Chemical-vapor deposition of wear resistant hard coatings in the Ti-B-C-N system: Properties and metal-cutting tests, *Int. J. Refract. Met. Hard Mater.* 20 (2002) 143–149, [http://dx.doi.org/10.1016/S0263-4368\(02\)00013-6](http://dx.doi.org/10.1016/S0263-4368(02)00013-6).
- [10] A. Larsson, S. Rупpi, Microstructure and properties of Ti(C,N) coatings produced by moderate temperature chemical vapour deposition, *Thin Solid Films* 402 (2002) 203–210, [http://dx.doi.org/10.1016/S0040-6090\(01\)01712-6](http://dx.doi.org/10.1016/S0040-6090(01)01712-6).
- [11] J. Garcia, R. Pitonak, R. Weissenbacher, A. Köpf, Production and characterization of wear resistant Ti(C,N) coatings manufactured by modified chemical vapor deposition process, *Surf. Coat. Technol.* 205 (2010) 2322–2327, <http://dx.doi.org/10.1016/j.surfcoat.2010.09.013>.
- [12] H. Chien, M.C. Gao, H.M. Miller, G.S. Rohrer, Z. Ban, P. Prichard, Y. Liu, Microtexture and hardness of CVD deposited α-Al₂O₃ and TiC_xN_{1-x} coatings, *Int. J. Refract. Met. Hard Mater.* 27 (2009) 458–464, <http://dx.doi.org/10.1016/j.ijrmhm.2008.09.010>.
- [13] C. Björmander, Coated Cutting Tool and Method of Manufacturing the Same, EP 2 604 720 A1, (2013).
- [14] S. Canovic, B. Ljungberg, C. Björmander, M. Halvarsson, CVD TiC/alumina and TiN/alumina multilayer coatings grown on sapphire single crystals, *Int. J. Refract. Met. Hard Mater.* 28 (2010) 163–173, <http://dx.doi.org/10.1016/j.ijrmhm.2009.08.001>.
- [15] S. Canovic, B. Ljungberg, M. Halvarsson, CVD TiC/alumina multilayer coatings grown on sapphire single crystals, *Micron* 42 (2011) 808–818, <http://dx.doi.org/10.1016/j.micron.2011.05.003>.
- [16] J. Herzler, P. Roth, High-temperature decomposition of TiCl₄ based on Cl-concentration measurements, *Proc. Combust. Inst.* 29 (2002) 1353–1359, [http://dx.doi.org/10.1016/S1540-7489\(02\)80166-3](http://dx.doi.org/10.1016/S1540-7489(02)80166-3).
- [17] E.A. Haupfear, L.D. Schmidt, Kinetics and multiple steady states in the chemical vapor deposition of titanium carbide, *J. Electrochem. Soc.* 140 (1993) 1793–1801.
- [18] G. Aylward, T. Findlay, *SI Chemical Data*, 5th ed, John Wiley & Sons Australia, Ltd, Milton, 2002.
- [19] H.E. Rebenne, D.G. Bhat, Review of CVD TiN coatings for wear-resistant applications: deposition processes, properties and performance, *Surf. Coat. Technol.* 63 (1994) 1–13, [http://dx.doi.org/10.1016/S0257-8972\(05\)80002-7](http://dx.doi.org/10.1016/S0257-8972(05)80002-7).
- [20] A. Kafizas, C.J. Carmalt, I.P. Parkin, CVD and precursor chemistry of transition metal nitrides, *Coord. Chem. Rev.* 257 (2013) 2073–2119, <http://dx.doi.org/10.1016/j.ccr.2012.12.004>.
- [21] A. Sherman, Growth and properties of LPCVD titanium nitride as a diffusion barrier for silicon device technology, *J. Electrochem. Soc.* 137 (1990) 1892–1897, <http://dx.doi.org/10.1149/1.2086826>.
- [22] H.H. Huang, M.H. Hon, Effect of N₂ addition on growth and properties of titanium nitride films obtained by atmospheric pressure chemical vapor deposition, *Thin Solid Films* 416 (2002) 54–61, [http://dx.doi.org/10.1016/S0040-6090\(02\)00606-5](http://dx.doi.org/10.1016/S0040-6090(02)00606-5).
- [23] B. Nölång, Computer program Ekvalc 4.6, Örnäsåtra, S-74386 Bålinge, Sweden, (1982).
- [24] P. Stenberg, P. Sukkaew, I. Farkas, O. Kordina, E. Janzén, L. Ojamäe, Ö. Danielsson, H. Pedersen, Silicon chemistry in fluorinated chemical vapor deposition of silicon carbide, *J. Phys. Chem. C* 121 (2017) 2711–2720, <http://dx.doi.org/10.1021/acs.jpcc.6b10849>.
- [25] M. Birkholz, *Thin Film Analysis by X-Ray Scattering*, Wiley-VCH Verlag GmbH & Co. KGaA, Weinheim, 2006.
- [26] W.C. Oliver, G.M. Pharr, An improved technique for determining hardness and elastic modulus using load and displacement sensing indentation experiments, *J. Mater. Res.* 7 (1992) 1564–1583, <http://dx.doi.org/10.1557/JMR.1992.1564>.
- [27] I. Dreiling, A. Haug, H. Holzschuh, T. Chassé, Raman spectroscopy as a tool to study cubic Ti–C–N CVD coatings, *Surf. Coat. Technol.* 204 (2009) 1008–1012, <http://dx.doi.org/10.1016/j.surfcoat.2009.05.029>.
- [28] F. Odell, Phase relationships in the binary systems of nitrides and carbides of zirconium, columbium, titanium, and vanadium, *J. Electrochem. Soc.* 97 (1950) 299–304.
- [29] J. Emmerlich, H. Högberg, S. Sasvári, P.O.Å. Persson, L. Hultman, J.P. Palmquist, U. Jansson, J.M. Molina-Aldareguia, Z. Czigány, Growth of Ti₃SiC₂ thin films by elemental target magnetron sputtering, *J. Appl. Phys.* 96 (2004) 4817–4826, <http://dx.doi.org/10.1063/1.1790571>.
- [30] T. Törndahl, J. Lu, M. Ottosson, J.-O. Carlsson, Epitaxy of copper on α-Al₂O₃(001) by atomic layer deposition, *J. Cryst. Growth* 276 (2005) 102–110, <http://dx.doi.org/10.1016/j.jcrysgro.2004.10.153>.
- [31] S.J. Bull, D.G. Bhat, M.H. Staia, Properties and performance of commercial TiCN coatings. Part 1: coating architecture and hardness modelling, *Surf. Coat. Technol.* 163–164 (2003) 499–506, [http://dx.doi.org/10.1016/S0257-8972\(02\)00650-3](http://dx.doi.org/10.1016/S0257-8972(02)00650-3).
- [32] D.R. Stull, H. Prophet, *JANAF Thermochemical Tables*, 2nd ed (NSRDS-NBS 37), 2nd ed, US Govt. Printing Office, Washington, 1971.
- [33] M.K. Karapet'janc, M.L. Karapet'janc, *Thermodynamic Constants of Inorganic and Organic Compounds*, Ann Arbor Humphery Science Publ, Ann Arbor, 1970.
- [34] K.K. Kelley, *U.S. Bur. Mines Bull.* 584 (1961), p. 592.
- [35] M.W. Chase, J.L. Curnutt, A.T. Hu, A.N. Syverud, L.C. Walker, *JANAF Thermochemical Tables*, 1974 Supplement, (1974), <http://dx.doi.org/10.1063/1.3253143>.
- [36] I. Barin, O. Knacke, O. Kubaschewski, *Thermochemical Properties of Inorganic Substances*, Supplement, Springer, Berlin, 1977.
- [37] O. Kubaschewski, C.B. Alcock, *Metallurgical Thermochemistry*, 5th ed., Pergamon Press, 1979.
- [38] D.D. Wagman, Selected values of chemical thermodynamic properties, *NBS Technical Notes*, 270-3, 270-4 and 270-5, U.S Govt. Printing Office, Washington, 1968.
- [39] B.A. Younglove, Erratum: thermophysical properties of fluids. I. Argon, ethylene, parahydrogen, nitrogen, nitrogen trifluoride, and oxygen, *J. Phys. Chem. Ref. Data* 14 (1985) 619, <http://dx.doi.org/10.1063/1.555731>.